A cortico-collicular circuit for accurate orientation to shelter during escape

Ruben Vale[1,2,#], Dario Campagner[1,3,#], Panagiota Iordanidou[1], Oriol Pavón Arocas[1], Yu Lin Tan[1], A. Vanessa Stempel[1], Sepideh Keshavarzi[1], Rasmus S. Petersen[4], Troy W. Margrie[1], Tiago Branco[1,*]

[1] UCL Sainsbury Wellcome Centre for Neural Circuits and Behaviour, London, W1T 4JG, UK

[2] MRC Laboratory of Molecular Biology, Cambridge, CB2 0QH, UK

[3] UCL Gatsby Computational Neuroscience Unit, London W1T 4JG, UK

[4] Division of Neuroscience & Experimental Psychology, University of Manchester, Manchester M13 9PT, UK

[#] Equal contribution

* For correspondence: t.branco@ucl.ac.uk

When faced with predatorial threats, escaping towards shelter is an adaptive action that offers long-term protection against the attacker. From crustaceans to mammals, animals rely on knowledge of safe locations in the environment to rapidly execute shelter-directed escape actions[1–3]. While previous work has identified neural mechanisms of instinctive escape[4–9], it is not known how the escape circuit incorporates spatial information to execute rapid and accurate flights to safety. Here we show that mouse retrosplenial cortex (RSP) and superior colliculus (SC) form a monosynaptic circuit that continuously encodes the shelter direction. Inactivation of SC-projecting RSP neurons decreases SC shelter-direction tuning while preserving SC motor function. Moreover, specific inactivation of RSP input onto SC neurons disrupts orientation and subsequent escapes to shelter, but not orientation accuracy to a sensory cue. We conclude that the RSC-SC circuit supports an egocentric representation of shelter direction and is necessary for optimal shelter-directed escapes. This cortical-subcortical interface may be a general blueprint for increasing the sophistication and flexibility of instinctive behaviours.

Escaping to shelter has higher survival value than simply moving away from the source of threat[10]. Refuges are places where predators are usually impeded from entering and where predation risk is thus very low[11]. To minimise exposure to the predator, navigating to the destination should in principle be as fast as possible[12], and animals rely on knowledge of the spatial environment to deploy accurate shelter-directed flights with very short reaction times[1,3]. Mice

in new environments can learn the location of a shelter within minutes, and when exposed to imminent threat orient in the shelter direction before running towards it along a straight vector[3]. Previous work has shown that shelter-directed escapes do not depend on sensory cues from the shelter and instead, mice use memory of the shelter location to reach to safety[1,3]. Rodents therefore rely on continuously keeping track of shelter direction during exploration to execute fast escape actions when exposed to threat[3,13,14]. Despite extensive knowledge about the neurobiology of spatial navigation[15–18], it is not known how the escape circuit accesses information about safe locations to generate accurate shelter-directed actions during escape.

To investigate this problem, we allowed mice to explore a circular arena with a shelter and presented innately threatening sound stimuli[19]. These reliably elicited shelter-directed escapes initiated with a head rotation movement that oriented the mouse in the shelter direction (Fig. 1A, Supplementary Video 1;[3]). To understand the neural basis of this action we focused on two brain regions: the retrosplenial cortex (RSP), which has been shown to encode representations of space, including head direction[20–22], goal[23], reward locations[24] and self-motion signals[20,25–27]; and the superior colliculus (SC), which can generate orienting motor commands[28–32] as well as escape initiation[4,33,34], and receives projections from the RSP[35–37]. By simultaneously recording single unit activity in these two regions while the animal explored the arena (Extended Data Fig. 1A; Supplementary Video 2; 836 RSP units, 683 SC units, 4 mice) we found that the firing rate of a subset of neurons in both the RSP and SC (centro- and latero-medial regions) is tuned to shelter direction (Fig. 1B,C; Supplementary Video 3; Extended Data Fig. 1B,C). This information is encoded in an egocentric frame of reference and represents the angle between the current heading and the shelter direction (Supplementary Video 3). The preferred tuning of these shelter-direction neurons covers the entire egocentric angular space (Fig. 1C, Extended Data Fig. 1C,D) and their firing rate is independent from allocentric head direction (Extended Data Fig. 1E, Extended Data Fig. 2). To confirm that the firing fields of shelter-direction neurons are anchored to the shelter, we rotated its position by 90 degrees while keeping all other landmarks in place, which resulted in escapes to the new location after a brief exploration period[3] (Fig. 1B; Supplementary Video 4). The firing fields rotated with the shelter and therefore maintained their angular tuning profile with respect to the shelter position (RSP median rotation=113°, IQR=[83°, 134°]; SC median rotation=99°, IQR=[83°, 127°]; P>0.9 vs 90° and P=0 vs 0°, *non-uniformity v-test*; Fig. 1D), indicating that neurons in RSP and SC specifically and dynamically encode the shelter direction.

The tuning of shelter-direction neurons could in principle reflect either a behaviourally relevant or perceptually salient location in the environment. To distinguish between these two possibilities, we added to the arena a second, identical shelter but with the entrance closed. Mice preferentially explored the open and closed shelters locations (Extended Data Fig. 1F), and threat presentation resulted in 79% escapes to the open shelter, 14% to the closed shelter and none to the LED (N=29 trials; Fig. 1E), indicating the relative behavioural relevance of each location for escaping from imminent threat. We then computed the egocentric direction tuning to these two locations, as well as to the

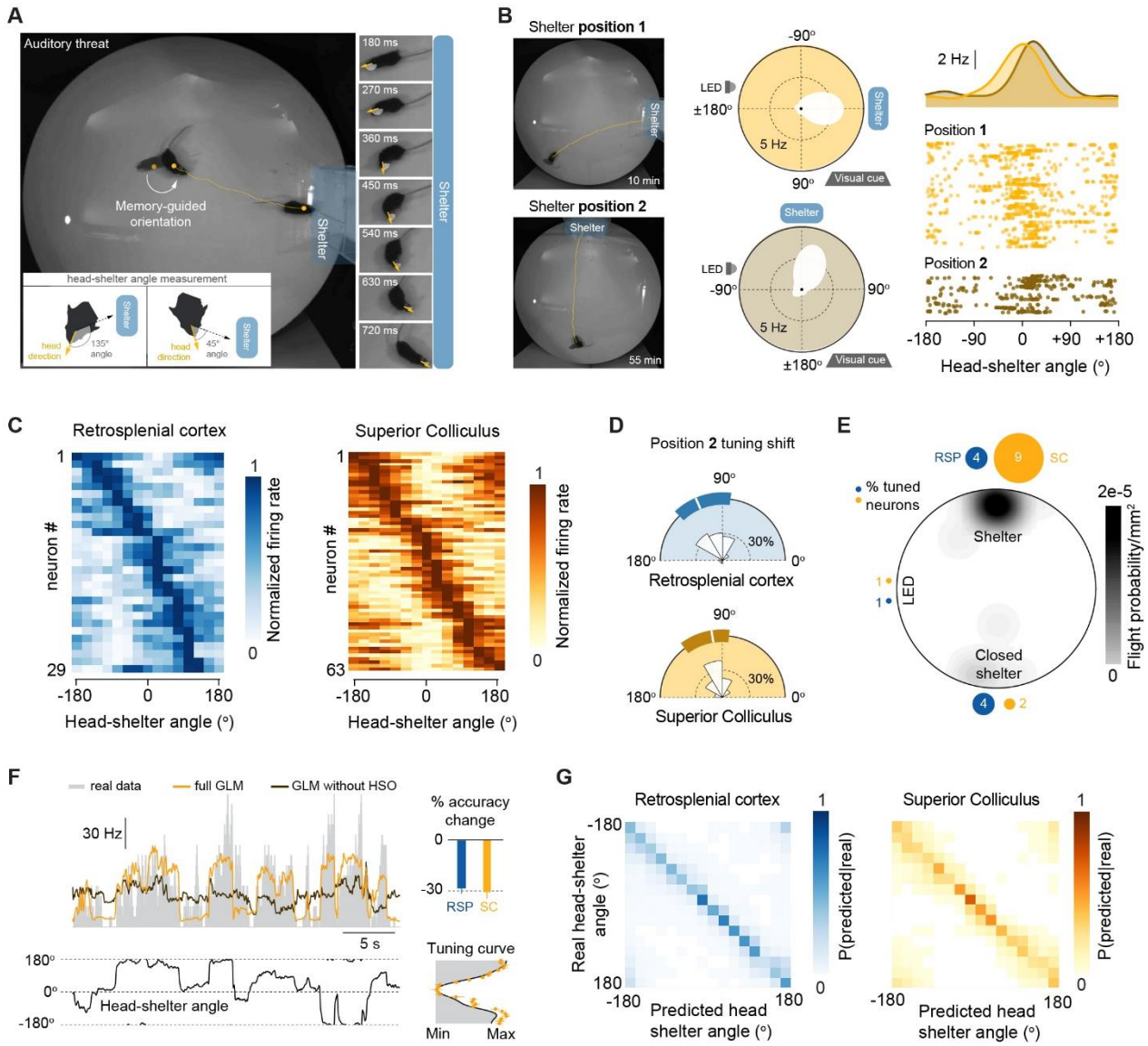

Figure 1 - RSP and SC neurons encode egocentric shelter direction

(A) Left, superimposed video frames showing orientation to shelter after a threat stimulus and subsequent shelter-directed escape (yellow line shows flight trajectory); inset illustrates measurement of egocentric shelter direction (defined as the head-shelter angle). Right, video frame sequence detailing the decrease in head-shelter angle at escape initiation (yellow arrows: head direction, white shade: head-shelter angle). **(B)** Left, video frames with escape trajectories (yellow lines) to initial shelter position (top, position 1) and after rotation (bottom, position 2). Centre, tuning curves for a single SC unit, showing a rotation of the firing field that follows the rotation of the shelter position. Other explicit landmarks remain in place (LED and visual cue). Right, sample raster plot and tuning curve for the same neuron. **(C)** Tuning curves for shelter-direction RSP and SC units for the shelter in position 1. Curves sorted by tuning peak. **(D)** Distribution of change in the Rayleigh vector direction after rotating the shelter by 90° (position 1 to position 2). **(E)** Schematic of flight termination probability across the arena and percentage of units tuned to each of the shelters and the LED landmarks (circle area is proportional to percentage).**(F)** Example GLM data for a SC neuron showing the evolution of recorded firing rate (top-left) and head-shelter angle (bottom-left), together with the full model fit (cross validated prediction accuracy: 50±3%) and the same model without the head-shelter angle variable. Bottom right shows the tuning curve recovered from the full model fit (yellow symbols) and the recorded curve (gray). **(G)** Cross-validated confusion matrices for LDA population decoding of head-shelter angle.

location of one the landmarks in the arena, a bright LED. While the fraction of RSP neurons tuned to the open and closed shelter was similar (open shelter: 3.5%, closed shelter: 3.5%; P=0.721, *two-proportions z-test*), SC neurons were preferentially tuned to the open shelter (open shelter: 9.2%, closed shelter: 1.6%; P=0.000638, *two-proportions z-test*),

with both regions being significantly less sensitive to LED location (RSP: 0.8%, P=0.0277; SC: 1.1%, P=0.00254; *two-proportions z-test* vs open shelter; Fig. 1D). This suggests that, in this context, while the RSP contains a broader representation of familiar places in the arena, neurons in the SC preferentially encode the direction of the most behaviourally salient location for escape.

Neurons in the SC and RSP have been shown to encode a range of different behavioural variables[38–41], so we next quantified the contribution of shelter tuning to the firing rate of shelter-direction neurons in both areas. We built a generalised linear model that included several variables, including head-direction and egocentric head movements (see Methods), and measured the difference in firing rate prediction accuracy between the full model and one without shelter direction (Fig. 1F). Removing the shelter-direction predictor caused a ~30% drop in prediction accuracy, confirming that this variable is a key determinant of firing rate in single RSP and SC neurons (relative accuracy drop: RSP=-24±3.67%, P=1.2511e-06; SC=-31± 3.6%, P=8.8599e-12, *one-tailed t-test*). Furthermore, at the population level, a linear discriminant analysis-based decoder (LDA) could use the neuronal firing rates to predict the shelter direction significantly above chance (prediction accuracy: SC=0.73, RSP=0.83; chance=0.19; Fig 1G). Together these results show that there are neurons in the RSP and SC that represent the ongoing shelter direction in an egocentric reference frame, which is the information needed to generate orienting movements towards the shelter during escape.

As the RSP is a hub for integrating spatial information upstream of the SC[40–42], we hypothesised that the representation of shelter-direction in the SC might depend on RSP input. We first characterised the anatomy of the RSP-SC projection[35–37] with cell type-specific monosynaptic retrograde rabies tracing[43] from VGluT2$^+$ and VGAT$^+$ starter cells (Fig. 2A; N=5 mice). Rabies injection of both SC populations resulted in prominent labelling of L5 RSP neurons, showing that both excitatory and inhibitory SC cells receive RSP input (Fig. 2A). Next, we measured the physiological properties of RSP-SC connections using whole-cell recordings *in vitro* and channelrhodopsin-2 expressed in the RSP. Optogenetic activation of RSP axons over the centromedial and centrolateral SC revealed a high connectivity rate for both excitatory and inhibitory SC neurons (VGluT2$^+$: 37.1%, N=70 cells, 4 mice; VGAT$^+$: 43.8%, N=73 cells, 4 mice). RSP input elicited excitatory monosynaptic potentials in both cell populations, and we found that temporal summation was more efficient in VGAT neurons because of differences in intrinsic excitability and short-term synaptic plasticity (Fig. 2B, C; Extended Data Fig. 3; 5th pulse peak voltage: 154±14% for VGAT$^+$, 79±12% for VGluT2$^+$, P=2.53e-4 *t-test*). Together, these data show that the SC directly receives significant synaptic input from the RSP.

To directly test whether the SC relies on RSP activity to encode shelter direction we assessed the effect of inactivating RSP neurons on SC shelter direction tuning. We used a retrograde AAV strategy[44] to express the inhibitory designer receptor hM4Di in SC-projecting RSP neurons (Fig. 2D) and measured the effect of i.p. CNO on RSP and SC

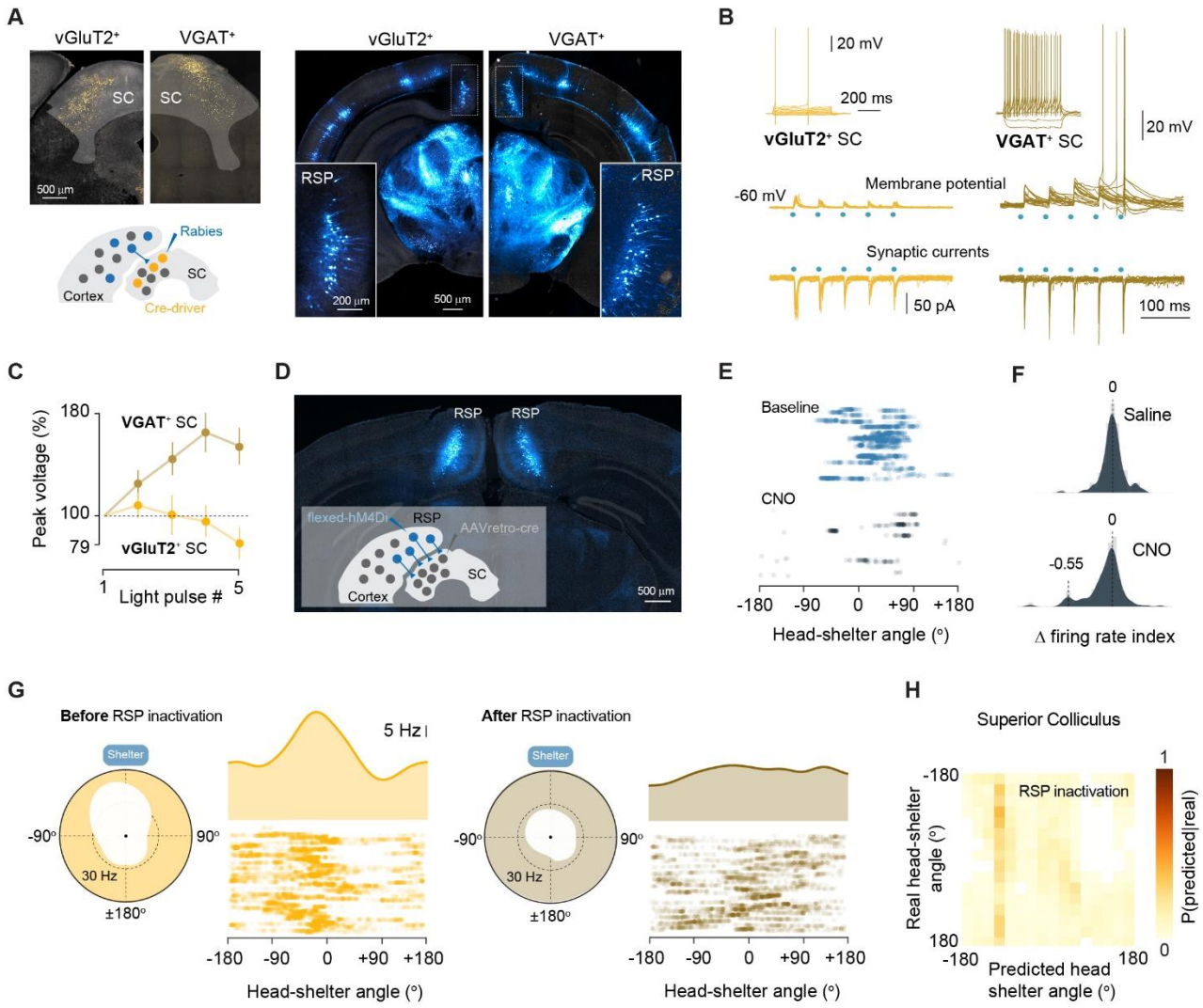

Figure 2 - Shelter-direction tuning in SC depends on RSP input

(A) Left, monosynaptic rabies tracing schematic (bottom) and coronal image of starter cells in the SC (top). Right, coronal image showing labelled input areas onto excitatory and inhibitory SC neurons, including the RSP (inset). **(B)** Example synaptic currents and potentials evoked by 20 Hz optogenetic stimulation of RSP inputs onto excitatory and inhibitory SC neurons (blue circles indicate stimulation times). Top inset shows voltage response to step current injections. **(C)** Summary plot of summation during 20 Hz optogenetic activation of RSP inputs (VGAT+: slope=17.6%, P=5.2e-13; VGluT2+: slope=-2.9%, P=0.16, linear regression). **(D)** Schematic of retrograde AAV strategy for inactivating SC-projecting RSP neurons, and coronal image of targeted RSP neurons. **(E)** Sample raster plot of an RSP shelter-direction cell before and after i.p. CNO. **(F)** Population histograms showing a decrease in firing rate in RSP neurons after i.p. CNO (see methods for index calculation). **(G)** Example tuning curves and sample raster plots showing loss of tuning in an SC shelter-direction neuron after i.p. CNO. **(H)** Cross-validated confusion matrix for LDA population decoding of head-shelter angle in SC after RSP inactivation.

single unit activity. Activation of hM4Di significantly decreased the *in vivo* firing rate of RSP neurons (P=0.0029 *one-tailed Kolmogorov-Smirnov test*; N=340 units, 2 mice; Fig. 2E, F). In the SC, while the overall firing rate of the population was not affected (Extended Data Fig. 4), RSP loss-of-function caused a 33% decrease in the fraction of SC shelter-direction neurons (P=0.01, *Chi square test*; Fig. 2G). Accordingly, the ability to decode shelter direction at the SC population level was also compromised (Fig. 2H; median change in accuracy: -18.76%; IQR: [-15.7%, -19.7%], P=0.0020 *sign rank test*). These data show that the representation of egocentric shelter direction in the SC depends on

RSP input. They further suggest that the RSP-SC pathway might be a critical neural circuit element for navigating to shelter during escape.

To investigate the relevance of RSP neurons and their SC projections for shelter-directed escape behaviour, we used the retrograde AAV strategy to inactivate SC-projecting RSP neurons while monitoring behavioural responses to imminent threat. Loss-of-function of these RSP neurons caused mice to make larger errors in the orientation phase of escape (Fig. 3A, B; Supplementary Video 5; median escape error: CNO = 23°, 105 trials, 11 mice; saline=5°, 51 trials, 6 mice; P = 0.0153 *permutation test*) without affecting exploratory behaviour (Extended Data Fig. 5A-F) or escape vigour (Extended Data Fig. 5G). This resulted in flight trajectories that were not directed towards the shelter location and consequently, the probability of terminating the flight outside the shelter was 7.4 times higher than the control (P=0.0001 *two-proportions z-test*; Fig. 3C). Although these escapes after RSP-SC inactivation were often resumed and the shelter eventually found, the time to shelter was 50% longer that observed for the control (CNO: median=2.1s, IQR=[1.8s, 2.8s]; saline: median=1.4s, IQR=[1.1s, 1.7s]; P=0.0439 *permutation test*; Extended Data Fig. 5H). Furthermore, flights were aborted earlier when orientation errors were largest (Extended Data Fig. 5I), suggesting that mice might retain awareness of shelter direction but are unable to select the appropriate direction of travel, similar to topographic disorientation in humans with RSP lesions[45]. We observed the same orientation impairment after global inactivation of RSP with chemogenetics (Supplementary Video 6; Extended Data Fig. 6A) and muscimol (Supplementary Video 7; Extended Data Fig. 6B). However, chemogenetic loss-of-function of other SC-projecting cortical areas did not perturb shelter-directed escapes, confirming that orienting to shelter is particularly dependent on RSP function (Fig. 3F, Extended Data Fig. 6C-D, Extended Data Fig. 7). Next, we tested whether the orientation deficits were specifically due to loss of activity in RSP-SC synapses. Projection-specific chemogenetic inactivation of this pathway with local CNO infusion[46] (Fig. 3D; Supplementary Video 8; Extended Data Fig. 8) recapitulated the escape orientation errors of global RSP loss-of-function (Fig. 3E). In contrast, inactivation of a control projection from the RSP to anterior cingulate cortex did not affect escape behaviour (Fig. 3F; Supplementary Video 9), further supporting a unique role of RSP-SC inputs in orienting to shelter during imminent threat.

The necessity for RSP input to SC for orienting to shelter could in principle be specific to this action or result from a more generic SC impairment whereby RSP input is necessary for SC control of head movement. To distinguish between these two hypotheses, we first analysed whether RSP inactivation affected the relationship between the firing rate of SC neurons and head movements. As previously reported[32,47–49], we found SC neurons tuned to egocentric head displacements (Fig. 3G), from which upcoming angular head movements could be decoded at the population level (Extended Data Fig. 9A). Chemogenetic inactivation of SC-projecting RSP neurons did not affect motor tuning and the LDA prediction accuracy was not different between CNO and saline conditions (Fig. 3G, I; median change: 2.1%; IQR: [0.2%,3.2%], P=0.11 *sign rank test*). This suggests that SC motor function was not affected by CNO, and therefore one

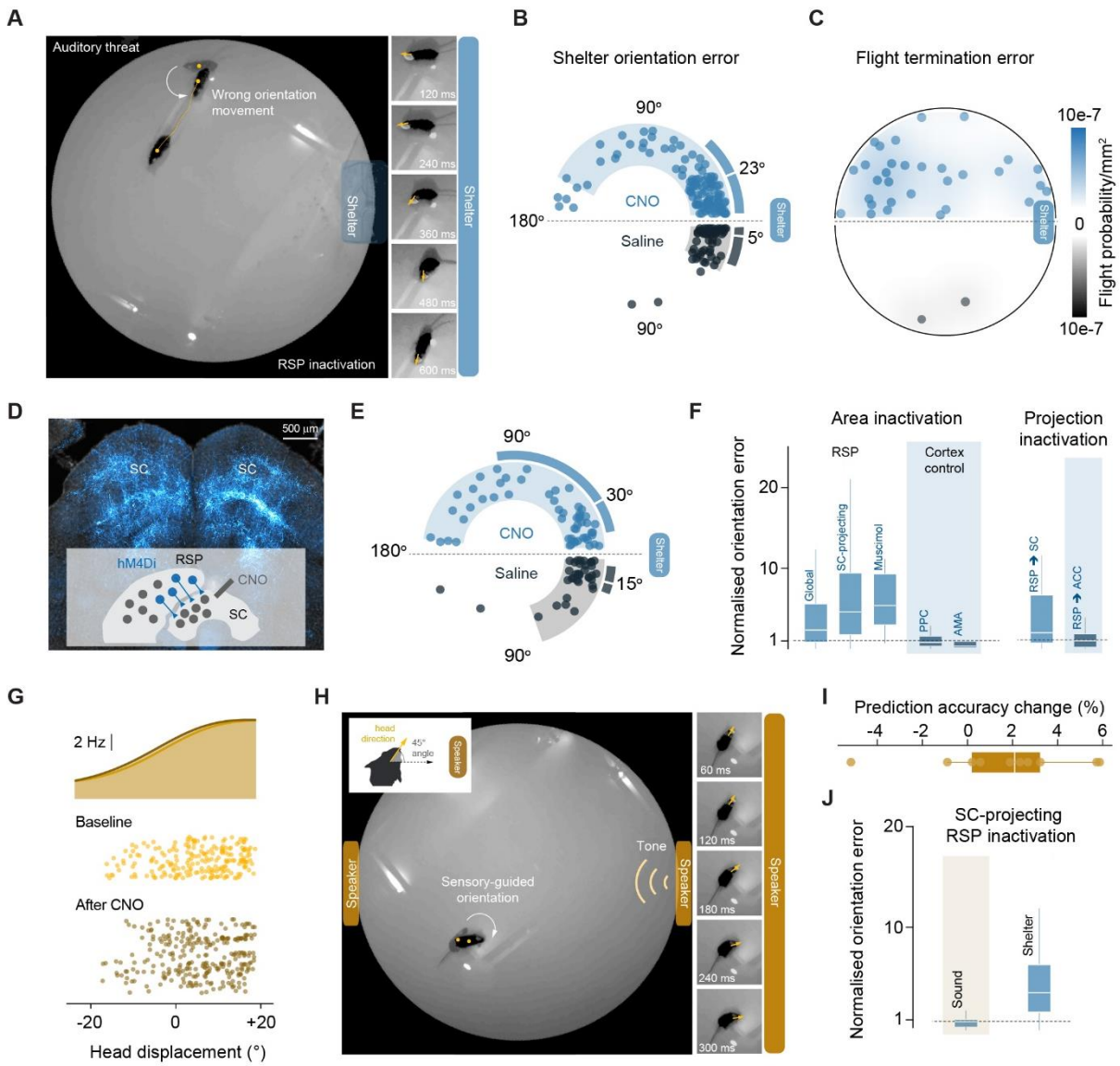

Figure 3 – RPS-SC input is specifically necessary to orient to shelter during escape

(**A**) Example video frames as in Fig. 1A showing escape initiation in the wrong direction due to incorrect orientation. (**B**) Summary plot of orientation errors at escape initiation after i.p. CNO. Light shaded area is 5-95 percentile range; dark bar is IQR and white line shows median. (**C**) Summary plot for location of flights terminated outside the shelter (CNO: 29.5%, saline: 3.9%). (**D**) Example coronal image of RSP axon terminals in the SC and schematic for local inactivation of these terminals.(**E**) Orientation errors as in B for local CNO infusion over SC (54 CNO trials, 37 saline trials, 6 mice; P=0.0032 permutation test). (**F**) Summary of activity manipulation effects on orientation errors. (Global RSP: 57 CNO trials, 5 mice and 32 saline trials, 5 mice, P=0.004; Muscimol: 21 muscimol trials, 6 mice and 25 saline trials 3 mice, P=0.0061; PPC: 31 CNO trials, 3 mice and 22 saline trials, 3 mice, P=0.6514; AMA: 31 CNO trials, 4 mice and 28 saline trials, 3 mice P=0.1003; RSP to ACC: 21 CNO trials, 5 mice and 21 saline trials, 5 mice, P=0.8282; permutation test). Data are normalized by dividing each inactivation trial error by the median of orientation error of the respective control dataset. (**G**) Tuning curve and sample raster plot for an SC neuron tuned to egocentric head displacement. (**H**) Example video frames showing instinctive orientation to a sound source. (**I**) Change in LDA prediction accuracy of head displacement from SC firing rates (% change in CNO - % change in saline). (**J**) Summary data showing no effect of RSP inactivation in the sound-orienting assay but increased shelter orientation errors for the same mice (P=0.0143 permutation test; 32 CNO trials and 42 saline trials). Data are normalized by dividing each CNO trial error by the median of orientation error of the respective control dataset.

prediction is that simple orientation movements to acute sensory stimuli should be preserved after RSP loss-of-function[50,51]. To test this prediction, we next developed a sound orienting assay to probe sensory-guided SC motor

function. One of two speakers placed opposite each other emitted a brief tone while the animal explored the arena. Mice innately oriented to the sound emitting speaker quickly and as accurately as they orient to the shelter (Fig. 3H; Extended Data Fig. 9B-E; Supplementary Video 10). However, in contrast to the shelter orientation errors during escape, inactivation of SC-projecting RSP neurons did not increase the error in orienting to the sound, confirming that RSP activity in not required for sensory stimulus-guided orientation (P=0.9290 *permutation test*; N=23 CNO trials and 26 saline trials, 4 mice; Fig. 3J; Supplementary Video 11).

Our results show that the RSP and SC continuously encode the egocentric direction of the shelter, with SC shelter-direction cells depending on RSP activity, and that the RSP-SC synaptic connection is necessary for accurate orientation to shelter during escape. A role for the RSP in representing egocentric shelter direction agrees with previous work showing that RSP neurons encode behaviourally important locations, such as landmarks, reward locations and a variety of spatial features of the environment[23–25,52,53]. In particular, the RSP integrates information from multiple streams to form representations of head-direction, place, and conjunctives of these variables[20,21,25,27,54], and it is thus well-positioned to compute spatial representations in egocentric coordinates[40–42]. A possible model therefore is that the RSP generates an egocentric representation of shelter direction that the SC inherits. Alternatively, our data might be indicative of a more general process whereby the RSP broadcasts spatial and self-motion signals, for example, which are used locally by the SC to assemble goal-relevant signals, such as shelter direction.

In our behavioural assay the shelter is a goal learned instinctively during exploratory behaviour, which mice escape to along a straight vector when exposed to imminent threat. The shelter-direction neurons we have found thus encode the angle of the escape goal vector in an egocentric reference frame. These neurons may be a dedicated subset for representing safe locations, but also be part of a population that can flexibly encode the direction of other types of goals, depending on the environment and motivation. The firing fields of shelter-direction cells are similar to goal-vector cells found in the hippocampus of bats[55] and the lateral entorhinal cortex of rats[56] navigating to learned reward locations, and to egocentric center-bearing cells in the postrhinal cortex[57]; though distinct from egocentric boundary vector cells[25,52,56,58,59]. Our recordings with two shelters in the arena further suggest that the RSP may form egocentric maps of behaviourally important locations in general. In contrast, the SC specifically encoded shelter direction. Together with the known role of the SC in establishing saliency and priority maps[60–62], these findings raise the possibility that the SC selects the most relevant goal-relevant target from a pool of RSP-encoded locations.

Previous work has demonstrated a role for cortico-collicular pathways mediating learned actions in highly trained animals in a variety of tasks and species[63–67]. Here we demonstrate that a cortico-collicular circuit is essential for an instinctive, survival behaviour. Given that SC motor function and sensory-guided orientation were not affected by RSP loss-of-function, our data suggest a selective role for RSP in the memory-guided orienting movements required to orient to shelter. This role might extend to other orienting actions that depend on memory of the target and which might

benefit from the hippocampal input onto RSP[68,69]. Future work will be needed to understand how the shelter orienting action is generated upon the detection of threat, which requires integrating additional information from areas such as the medial SC[8]. A possible advantage of this cortico-collicular organization is to use cortical circuits to perform complex computations and distil the result to variables that can be easily converted into actions – here, the shelter direction continuously mapped already in egocentric coordinates. This could potentially decrease the time to initiate the action, which in the case of escaping from imminent threat is of great survival value. The model that emerges from our results may therefore represent a generic brain strategy for using cortical output to generate fast and accurate goal-directed actions.

Experimental procedures

Mice

All experiments were performed under the UK Animals (Scientific Procedures) Act of 1986 (PPL 70/7652 and PFE9BCE39) following local ethical approval. Male adult C57BL/6J wild-type (Charles Rivers, 6 – 24 weeks old) were used for all behavioural experiments. Mice were single housed after surgery and at least 3 days before starting behavioural protocols. Mice had free access to food and water on a 12:12 h light:dark cycle and were tested during the light phase (unless stated otherwise). VGluT2::eYFP (resulting from in-house cross of VGluT2-ires-Cre with R26-stop-eYFP, JLS #016963 and #006148 respectively; JLS: Jackson Laboratory stocks) or VGAT::eYFP (resulting from in-house cross of VGAT-Cre with R26-stop-eYFP, JLS #016962 and #006148 respectively) mice (5 – 8 weeks old) were used for ChR2-assisted circuit mapping. VGluT2-ires-Cre (JLS #016963) or VGAT-Cre (JLS #016962) mice (9 – 20 weeks old) were used for retrograde rabies tracing.

Surgical procedures

Mice were anaesthetized with an intraperitoneal (i.p.) injection of ketamine (95 mg kg^{-1}) and xylazine (15.2 mg kg^{-1}) or with isoflurane (2.5% - 5%) and secured on a stereotaxic frame (Kopf Instruments). Carprofen (5 mg kg^{-1}) was administered subcutaneously for analgesia. Isoflurane (0.5–2.5% in oxygen, 1 l min^{-1}) was used to maintain anaesthesia. Craniotomies were made using a 0.5 mm burr and coordinates were measured from bregma or lambda (see Supplementary Tables 1 and 2 for implant affixation and virus injection coordinates, respectively). Viral vectors were delivered using pulled glass pipettes (10 µl Wiretrol II pulled with a Sutter-97) and an injection system coupled to a hydraulic micromanipulator (Narishige), at approximately 50 nl min^{-1}. Implants were affixed using light-cured dental cement (3M) and the surgical wound was sutured (Vicryl Rapide) or glued (Vetbond).

Viruses

The following viruses were used in this study and are referred to by contractions in the text. Chemogenetic projection-specific inhibition experiments: rAAV2-retro-CMV-bGlo-iCre-GFP (made in house; $1.07x10^{12}$ GC ml^{-1}; [44]) and AAV2-hSyn-DIO-hM4D(Gi)-mCherry (Addgene #44362; $4.6x10^{12}$ GC ml^{-1}; [70]); chemogenetic non-projection specific inhibition experiments AAV8-hSyn-hM4D(Gi)-mCherry (Addgene #50475; $4.8x10^{12}$ GC ml^{-1}). Retrograde rabies tracing[43]: EnvA pseudotyped SADB19 rabies virus (SAD-B19$^{\Delta G}$-mCherry; made in house; $2x10^{8}$ GC ml^{-1}) used in combination with AAV1 encoding the EnvA receptor TVA and rabies virus glycoprotein (prepared in house from AAV1-Flex-N2cGnucGFP, $7x10^{12}$ GC ml^{-1}) and AAV1-EF1a-Flex-GT-GFP (made in house ; $2x10^{12}$ GC ml^{-1}); ChR2-assisted circuit mapping: AAV1-CAG-hChR2(H134R)-mCherry-WPRE-SV40 (Penn Vector Core; $2x10^{14}$).

Behavioural procedures

Experimental setup

All behavioural experiments were performed in an elevated circular Perpex arena (92 cm diameter), located in an opaque, sound-deadening 140 x 140 x 160 cm enclosure[3]. The shelter was an over-ground red translucent Perspex box (20 x 10 x 10 cm) placed at the edge of the arena, with a 4.2 cm wide entrance facing the centre of the arena. The enclosure held six infrared light-emitting diodes (LED) illuminators (Abus) and experiments were recorded with an overhead near-IR GigE camera (Basler), at 30 or 40 frames per second. Unless stated otherwise, experiments were conducted at a background luminance of 2.7 lux, generated by a projector (BenQ) pointed at a translucent overhead screen (Xerox). Video recording and sensory stimulation (see below) were controlled with custom software written in LabVIEW (2015 64-bit, National Instruments) and Mantis software (mantis64.com). All signals and stimuli, including each camera frame, were triggered and synchronised using hardware-time signals controlled with a PCIe-6351 and USB-6343 board (National Instruments).

Sensory stimuli

Escape behaviour assay: The stimulus was a frequency-modulated auditory upsweep from 17 to 20 kHz over 2 s [19]. In a small fraction of experiments additional stimuli were used to minimise habituation of escape responses. Waveform files were created in MATLAB (Mathworks), and the sound was generated in LabVIEW, amplified and delivered via an ultrasound speaker (Pettersson) positioned 50 cm above the arena centre. Sound pressure level at the arena floor was 73 - 82 dB. Orientation to sound assay: The stimulus was a 300 ms tone at a frequency of 2.5 kHz. Sound pressure measured at the centre of the arena was 75 – 80 dB.

Behavioural protocols

Escape behaviour assay: the procedure was conducted as previously described [3]. Before the experiment, bedding from the animal's home cage was placed inside the shelter. After a 7 min habituation period, during which the mouse had to enter the shelter at least once, sound stimuli were delivered. During a single session, multiple stimuli were delivered with an inter-stimulus interval of at least 90 s. Typically, half of the trials were presented in the dark (0.01 – 0.03 lux); escape error was not different between dark and light conditions and therefore the results were pooled ($P>0.05$ for all datasets *permutation test*). Experiments had a typical duration of 90 minutes.

Orientation to sound assay: experiments were conducted in the dark using the same arena as the escape behaviour assay. The stimulus was delivered by one of two speakers at the height of arena floor, 10 cm away from the edge and positioned at diametrically opposite sides. After a 7 min habituation period, 7 stimuli were presented with an inter-

stimulus interval of at least 90 s from a randomly selected speaker. Stimuli were typically presented when mice subtended an angle smaller than 120° towards the speaker because sound location in azimuthal plane has been shown to be unreliable above this range[71,72]. Experiments had a typical duration of 40 minutes.

Analysis

Behavioural video and tracking data were sorted into peri-stimulus trials and manually annotated. Detection of the stimulus was assed as previously described [4]. Escape behaviour assay: Onset of escape was determined by visual inspection of the video recordings and considered as either the onset of a head-rotation movement or an acceleration (whichever occurred first) after the mouse detected the stimulus[4]. Flight termination was defined as the first time the mouse stopped outside the shelter, re-oriented or arrived to shelter, after having initiated an escape. Escape error was computed as the head-shelter angle at the end of the orientation phase of escape (see Fig. 1A for example of an accurate orientation phase where escape error is close to 0°). Head-shelter angle was measured manually using a custom-designed Python-based graphic interface and varied between 0° (mouse heading perfectly aligned to the centre of the shelter entrance) and ±180° (positive angles are measured in the clockwise direction from the shelter, negative angles are measured in the anti-clockwise direction). Flight distance was computed as the ratio of the Euclidean distance between the mouse position at escape onset and at the flight termination, over the Euclidean distance between the mouse position at escape onset and the shelter entrance. Orientation to sound assay: Orientation error was computed as the head–speaker angle at the end of the first orientation movement after the auditory stimulus presentation..

Pharmacological inactivation

Mice were bilaterally implanted with guide and dummy cannulae (Plastics One) over RSP and given at least 96 h for recovery. On experiment day, the animals were infused with 1.0 – 1.2 µL Muscimol-BODIPY-TMR-X (0.5mg/ml, ThermoFisher) or vehicle per hemisphere and tested in the escape behaviour assay. Mice were anesthetised and internal cannulae projecting 0.5 mm below guide cannulae, were inserted and sealed with Kwik-Sil. Muscimol or vehicle were then infused at a rate of 150–200 nl min^{-1} using a microinjection unit (Hamilton, 10µl syringe; in Kopf Instruments Model 5000) connected to the internal canula through tubing (Plastics One) and a plastic disposable adaptors (Plastics One). Mice were given 35 minutes to recover before starting the escape behaviour assay.

To confirm infusion site, immediately upon termination of the behavioural assay, mice were anaesthetized with isoflurane (5%, 2 l min^{-1}) and decapitated. The brain was sectioned coronally (100 µm) with a vibrotome (Campden Instruments) in ice-cold PBS (0.1 M), directly transferred to 4% paraformaldehyde (PFA) solution, and kept for 20 min

at 4 °C. The slices were then rinsed in PBS, counter-stained with 4′,6-diamidino-2-phenylindole (DAPI; 3 μM in PBS), and mounted on slides in SlowFade Gold (Thermo Fisher) before imaging (Zeiss Axio Imager 2) on the same day.

Chemogenetic inactivation

Mice were injected with a retro-AAV (rAAV2-retro-CMV-bGlo-iCre-GFP) into the SC and AAV2-hSyn-DIO-hM4D(Gi)-mCherry into the RSP for projection-specific inactivation, or with AAV8-hSyn-hM4D(Gi)-mCherry into the target locations for global inactivation. After at least 4 weeks mice were intraperitoneally injected with CNO (final concentration of 10 mg kg^{-1}; Hellobio CNO freebase) or saline, during brief (<2 min) isoflurane anaesthesia (2 – 4% in oxygen, 1 L min^{-1}). Mice were given 35 minutes to recover before starting behavioural experiments. Saline and CNO sessions for a given mouse were spaced in time at least 3 days. In a subset of the above mice, cannulae were implanted either in the SC or in the anterior cingulate cortex (ACC) to inactivate specifically the respective RSP projection[46]. Guide and dummy cannulae (Plastics One) were implanted into the target location at least 4 weeks after viral injection, and at least 4 days before behavioural experiments. Cannulae implantation and infusion were performed as described in the *Pharmacological inactivation experiment* section. CNO was diluted in buffered saline containing (in mM): 150 NaCl, 10 D-glucose, 10HEPES, 2.5 KCl, 1 MgCl2 and to a final concentration of 10 μM. 0.8 – 1.2 μL of CNO were infused.

Anatomical tracing

Injections for monosynaptic rabies tracing[43] from unilateral $VGluT2^+$ or $VGAT^+$ SC cells were performed with an angled approach to avoid infection of the ipsilateral RSP. In the first surgery, a mix of AAV1-Flex-N2cGnucGFP24 and AAV1-EF1a-Flex-GT-GFP25 was injected in the left SC (10° ML angle; AP: -0.40 mm from lambda; ML: -1.00 mm; DV: -1.75 mm; injection volume = 20 -25 nL). SAD-B19DG-mCherry rabies virus was injected vertically 5 days after the first procedure (same target location; injection volume = 25 – 30 nL). Mice were perfused 10 days after the second procedure. Brains were imaged by serial micro-optical sectioning 2-photon tomography[73] (40 μm thick coronal sections; voxel size ML 2 μm, DV 2 μm, AP 5 μm). Images were inspected visually, and projections of interest were identified in reference to the Allen Mouse Brain Atlas (c 2015 Allen Institute for Brain Science. Allen Brain Atlas API. Available from: brain-map.org/api/index.html). One sample brain was sectioned using a cryostat (Leica 3050 S) and imaged with an epifluorescence microscope (Zeiss Axio Imager 2)

***in vitro* whole-cell recordings**

Preparation of acute midbrain slices

Male and female VGluT2::EYFP or VGAT::EYFP mice were injected with AAV1-CAG-hChR2(H134R)-mCherry-WPRE-SV40 in RSP. After 2 weeks mice were killed by decapitation following isoflurane anaesthesia. Brains were quickly removed and immediately immersed in ice-cold slicing solution containing (in mM): 87 NaCl, 2.5 KCl, 26 $NaHCO_3$, 1.25 NaH_2PO_4, 10 glucose, 50 sucrose, 0.5 $CaCl_2$, and 3 $MgCl_2$, with an osmolarity of 281-282 mOsm, and constantly bubbled with carbogen (95% O_2 and 5% CO_2) for a final pH of 7.3. Acute coronal slices of 250 µm thickness were prepared at the level of the SC (-0.8 to 0.2 mm from lambda) using a Vibratome (Leica VT1200 S). Slices were collected and transferred to a recovery chamber containing slicing solution and stored under submerged conditions at near-physiological temperature (35°C) for 30 minutes, constantly bubbled with carbogen (95% O_2 and 5% CO_2). Slices were then transferred to a different recovery chamber and submerged in artificial cerebrospinal fluid (aCSF) solution containing (in mM): 125 NaCl, 2.5 KCl, 26 $NaHCO_3$, 1 NaH_2PO_4, 10 glucose, 2 $CaCl_2$, and 1 $MgCl_2$, with an osmolarity of 293-298 mOsm and constantly bubbled with carbogen (95% O_2 and 5% CO_2) for a final pH of 7.3. Slices were further incubated at room temperature (19-23 °C) for at least 30 more minutes prior to electrophysiological recordings.

Recording electrodes

Pipettes were pulled from standard-walled filament-containing borosilicate glass capillaries (Harvard Apparatus, 1.5 mm OD, 0.85 mm ID) using a vertical micropipette puller (PC-10 or PC-100, Narishige) to a final resistance of 4-6 MΩ. Pipettes were backfilled with potassium methane sulfonate based solution containing (in mM): 130 $KMeSO_3$, 10 KCl, 10 HEPES, 4 NaCl, 4 Mg-ATP, 0.5 Na_2-GTP, 5 Na-Phosphocreatine, 1 EGTA, biocytin (1 mg mL^{-1}), with an osmolarity of 294 mOsm, filtered (0.22 µm, Millex) and adjusted to pH 7.4 with KOH.

Data acquisition

Whole-cell patch-clamp recordings were performed with an EPC 800 amplifier (HEKA). Data were sampled at 25 kHz, low-pass Bessel filtered at 5 kHz, digitised with 16-bit resolution using a PCIe-6353 board (National Instruments) and recorded in LabVIEW using custom software. For recordings, slices were transferred to a submerged chamber and perfused with aCSF constantly bubbled with carbogen (95% O_2 and 5% CO_2). The solution was perfused at a flow rate of 2-3 ml/min with a peristaltic pump (PPS2, MultiChannel Systems or Minipuls 3, Gilson) and temperature was kept at 32-34°C. Expression of ChR2-tdTomato was assessed based on fluorescence from tdTomato expression using LED illumination (pE-100, CoolLED) at a wavelength of 565 nm. Cells were visualised with oblique illumination on an upright SliceScope Pro 1000 (Scientifica) using a 60x water-immersion objective (Olympus) or with DIC illumination on an upright SliceScope Pro 6000 (Scientifica) using a 40x water-immersion objective (Olympus). Target cells were identified based on fluorescence from EYFP expression using LED illumination (pE-100, CoolLED) at a wavelength of

490 nm. The resting membrane potential was determined immediately after establishing the whole-cell configuration and experiments were continued only if cells had a resting membrane potential more hyperpolarized than −45 mV. Input resistance (*R*in) and series resistance (*R*s) were monitored continuously throughout the experiment, and *R*s was compensated in current-clamp recordings. Only cells with a stable *R*s < 40 MΩ were analysed. ChR2 was activated with wide-field 490-nm LED illumination (pe-100, CoolLED, 1-ms pulse length, 5 pulses at 20 Hz, maximum light intensity = 6 mW). Upon termination of the recording, the anatomical location of the neuron within the slice was recorded using a 5x objective (Olympus) for future reference. After the experiment, slices were fixed with 4% PFA for 2 hours, kept in 4°C PBS overnight, and imaged using an epifluorescence microscope (Zeiss Axio Imager 2).

Analysis

Analysis was performed in python 2.7. Normalised peak voltages of EPSPs in a train were calculated by dividing the peak amplitude of each evoked EPSP to the first evoked EPSP. Membrane potential values stated in the text are not corrected for liquid junction potentials.

Histological procedures

For general histology mice were anaesthetized with Euthatal (0.15–0.2 ml) and transcardially perfused with 10 ml of ice-cold PBS with heparin (0.02 mg ml−1) followed by 4% PFA in PBS solution. Brains were post-fixed overnight at 4 °C then transferred to PBS solution. Sections (50 µm) were cut with a cryostat (Leica CM3050S) and stained. Unless otherwise stated, sections were imaged with an epifluorescence microscope (Zeiss Axio Imager 2).

Immunohistochemistry was performed to enhance the signal of hM4D-mCherry-expressing RSP neurons. Sections were initially blocked using a 5% normal donkey serum (NDS) in PBS solution. Subsequently, they were incubated overnight at 4ºC with anti-RFP primary antibody (1:1000, rabbit; 600-401-379, Rockland), followed by a 2-hour incubation with Alexa-568 donkey anti-rabbit. Antibodies were diluted in 0.5% NDS and 0.05% Triton X-100. DAPI was used for counterstaining. Sections were mounted in SlowFade Gold (Thermo Fisher, S36936) onto slides before imaging.

Single unit recordings in freely moving animals

Data acquisition

Mice were singly housed after probe implantation in a reversed 12 h light cycle and tested during the dark phase of the day light cycle. One Neuropixels probe (phase3A, option1, 384 channels;[74]) was chronically implanted in the RSP and SC. Before insertion, the probe shank was coated with DiI (1 mM in ethanol, Invitrogen) for track identification (Extended Data Fig. 1A). At the end of the experiment the mouse was perfused and the brain was imaged with an

epifluorescence microscope (Zeiss AxioImager 2) or by serial micro-optical sectioning 2-photon tomography to confirm the location of probe implantation (see *Anatomical tracing* section). For single unit recording experiments paired with chemogenetic inactivation, probes were implanted in mice previously injected (4 weeks) with viruses as described in *Chemogenetic inactivation*.

Extracellular recordings in freely moving animals were performed in a similar behavioural apparatus as described in *Behavioural procedure*, with an over ground shelter (20 x 10 x 10 cm; 12 cm wide entrance) positioned by the edge and facing the centre of the platform. Two explicit visual cues were positioned in the environment: a yellow LED, always positioned on the 'West wall' of the behavioural cabinet, and an A2 white cardboard sheet, always positioned in the 'South wall' of the cabinet, both distal to the arena. A custom-made rotary joint (adapted from Doric AHRJ-OE_PT_AH_12_HDMI) was used to prevent the cables from twisting. Each mouse was tested multiple times with a minimum time interval between consecutive experiments of 3 days. During each session, the mouse explored the shelter in two locations (east pole of the arena: shelter position one; north pole of the arena: shelter position 2) for at least 30 minutes each. In a fraction of the experiments, after the mouse was tested in the protocol described above, the LED was moved to the east pole of the arena or a closed shelter was introduced at the south pole of the arena and then moved to the east pole. For Neuropixels recording experiments paired with chemogenetic inactivation, the intraperitoneal injection of CNO (or saline) was done during the behavioural experiment, after the mouse explored the shelter in the second position for at least 30 minutes. The mouse was not removed from the arena and was not anesthetised for the injection. Although the recording was never interrupted, the 35 minutes following the injection were excluded from further analysis. Extracellular potentials were recorded with SpikeGLX (https://github.com/ billkarsh/SpikeGLX, Janelia Research Campus) and were amplified (500 x), high-pass filtered (300 Hz) and sampled at 30 kHz.

Analysis

Data analysis was performed in MATLAB. Spike sorting was done using Janelia Rocket Cluster 3.0[75] or Kilosort 2.0[76] and manually curated. Only units that had an absolute refractory period of at least 1 ms were included in subsequent analysis. Behavioural variables were extracted from video recordings using DeepLabCut (DLC[77]; training set 1000 frames, 1 million training iterations). All timepoints during which the mouse was either inside the shelter or leaning down the behavioural platform where excluded from further analysis. Head-direction and head-shelter angle were calculated using DLC tracked ear-positions: head-direction was defined as the angle between the direction perpendicular to a line that joins both ears and the horizontal axis; head-shelter angle was defined as the angle between the same direction as above and a line connecting the centre point between the ears and the shelter entrance (Fig. 1A, Extended Data Fig. 2B, Supplementary Video 3).

Single cell tuning analysis: criteria for classification of shelter-direction and head-direction cells

We used Rayleigh vector length[78] in head-direction and head-shelter angle spaces, as previously described in head-direction tuning testing in rodents[79], to quantify the tuning of each cell to each of these variables. A neuron was considered to be significantly tuned to a variable when the length of its Rayleigh vector exceeded the 95th percentile of the distribution of Rayleigh vectors lengths computed for 1000 shuffled-datasets, generated by shifting recorded spike trains from all cells coherently by a uniform amount chosen randomly between 1 and 100 s. To ensure the tuning estimation was not influenced by potential behavioural biases, we binned the variable space into 16 bins and sampled them equally. Single units from RSP or SC were classified as shelter-direction cells if all the following criteria were met: i) for each epoch the neuron has to display a significant head-shelter angle Rayleigh vector; ii) for each epoch the neuron tuning to head-shelter angle must de decoupled from tuning to head-direction (using the Tuning Entanglement Decoupling (TunED) analysis, see below); iii) head-shelter angle tuning has to be stable across all epochs (above chance ROC decoding[80] along the direction in which Rayleigh vector points during the shelter position 1 epoch, in shelter position 2 epoch); iv) head-shelter angle tuning must rotate with the shelter (after rotation of the shelter, the tuning to shelter position 2 must not be significantly explained by the tuning to shelter position 1, using TunED analysis). Single units from RSP or SC were classified as head-direction cells if all the following criteria were met: i) for each epoch (including the no shelter epoch) the neuron had to display a significant head-direction Rayleigh vector; ii) for each epoch the neuron tuning to head-direction had to be decoupled from tuning to head-shelter angle (using the TunED method); iii) head-direction tuning has to be stable across all epochs (above chance ROC decoding along the direction in which Rayleigh vector points during the first epoch of the experiment, in the subsequent periods).

Tuning entanglement decoupling (TunED) analysis

To determine whether a neuron that is statistically tuned to two correlated variables is driven by just one of the variables (v_1, 'driver') while the tuning to the second variable (v_2, 'passenger') is an artefact of the correlation, we performed tuning entanglement decoupling analysis (TunED). The method takes a list of spike-counts r along with simultaneously measured stimulus variables v_1 and v_2 Let

$$P(r = i|v)$$

be the probability that the neuron's spike count r takes a given value, given a discrete value for the variable v, the tuning curve of the neuron to stimulus variable v (observed tuning to v_1 or v_2, Extended Data Fig. 2A, right panel, dark yellow and dark blue) is then the conditional mean spike count

$$\mu(v) = \sum_i i\, P(r = i|v)$$

To determine whether a neuron is only tuned to the driver variable v_1 or indeed significantly tuned to both v_1 and v_2, the method formulates the null hypothesis that the neuron's activity is purely driven by the v_1. In this case it can be shown that the tuning curve to v_2 ($\mu(v_2)$; expected tuning of v_2 given tuning to v_1, Extended Data Fig. 2A, right panel, light yellow and light blue) can be expressed as:

$$\mu_{NH}(v_2) = \int dv_1\, \mu(v_1) P(v_1|v_2)$$

Where the suffix *NH* denotes this is not the actual tuning curve to v_2 but instead it is derived by the above null hypothesis.

TunED analysis was used to classify cells has head direction or shelter-direction cells. Recorded spike and head direction and head shelter angle time series were bootstrapped 1000 times, generating 1000 observed tuning curves to each variable (Extended Data Fig. 2C, left panels, dark yellow and dark blue) as well as 1000 expected tuning curves of the same variable using the null-hypothesis equation above (Extended Data Fig. 2C, left panels, light yellow and light blue). For each variable, the Euclidean distance (d_{HSA} and d_{HD}) between the observed (OT_{HSA} and OT_{HD}) and the expected (ET_{HSA} and ET_{HD}) tuning curves was calculated for each bootstrap iteration (Extended Data Fig.2C, right panels, yellow and blue histograms). Finally, we computed the distribution of the differences between each variable d_{HSA} and d_{HD} for each bootstrap iteration (Extended Data Fig. 2C, right panels, dark grey histograms). If the distribution of d_{HSA} - d_{HD} was significantly smaller than zero (both 2.5^{th} and 97.5^{th} percentile <0, vertical dotted lines in Extended Data Fig. 2C, right panels) the cell was considered a head direction cell (Extended Data Fig. 2C, top panels); if the distribution of d_{HSA} - d_{HD} was significantly larger than zero (both 2.5^{th} and 97.5^{th} percentile > 0) the cell was considered a head-shelter angle cell (Extended Data Fig. 2C, bottom panels); otherwise the cell was not considered a head-shelter angle nor head direction cell.

Generalized linear model (GLM)

Generalized linear models[81] were used to predict the probability of spiking at certain time *t* during shelter position 1 and shelter position 2 epochs, given the values of a set of simultaneously recorded variables at time *t* (head-direction, head-shelter angle, locomotion velocity, head angular velocity, change in head direction within the next 100ms and 200ms; see [48]). For each of these variables we defined a set of equally spaced bins (locomotion speed, 11; head direction, 27; head-shelter angle, 27; head angular velocity, 23; change in head direction within the next 100ms, 13; change in head direction

within the next 200ms, 13). A time varying binary predictor was then defined for each bin (excluding one) of each variable. At a given *t*, each binary predictor could be 1, if the value of the respective behavioural variable fell in that bin at *t* and zero otherwise. The GLM was fitted with the *glmfit* MATLAB function assuming logistic link function and Bernulli probability distribution. Model prediction accuracy was assessed by performing 10-fold cross-validation and computing Pearson correlation coefficient between predicted and real spike trains (smoothed over 100 ms). The analysis above was also performed after excluding head-shelter angle from the model.

Population decoding analysis

We employed multiclass linear discriminant analysis (LDA; [82]) to decode head-shelter angle from spike trains of RSP and SC neural populations, and change in head direction within the next 100ms from spike trains of SC neural population. Head-shelter angle was binned into 16 equally populated classes (bin range: -180° to 180°, bin amplitude: 22.5°), and change in head direction into 9 classes (bin range: -27° to 27°, bin amplitude: 6°). Population data was constructed by grouping all recorded neurons and aligning their activity according to the value of head-shelter angle (or change in head direction) in which it was measured. Both shelter positions 1 and shelter positions 2 epochs were divided into 6 interleaved time periods of equal duration; for each epoch periods 1, 3 and 5 were used to train the classifier, while periods 2, 4 and 6 were used to test its accuracy. Prediction accuracy was computed as the fraction of observations of the testing set classified in the main diagonal of the classifier confusion matrix and in the adjacent ones (± 1), over the total number of observations in the testing set. Predictions accuracy was also compared to the one obtained for a shuffled dataset.

Single unit recordings paired with chemogenetic loss-of-function analysis

Firing rate change

The effect of inactivation was assessed separately in RSP and SC neurons. Change in firing rate index (Δ firing rate index) for each neuron in the period before (shelter position 2 epoch) and after the administration of CNO (or saline) was computed as:

$$\Delta Firing\ Rate\ index = \frac{firing\ rate_{after\ injection} - firing\ rate_{before\ injection}}{firing\ rate_{after\ injection} + firing\ rate_{before\ injection}}$$

Single cell analysis

To test for changes in the percentage of neurons classified as shelter-direction neurons we first identified shelter-direction as described above in the periods before and after the injection.

We then computed:

$$\frac{fraction_{CNO} - fraction_{sal}}{fraction_{sal}}$$

where *fraction* is the fraction of shelter-direction cells after the injection.

Population analysis

We computed the change in prediction accuracy of multiclass LDA classifiers (see *population decoding analysis*), following injection of CNO or saline in respect to baseline. The period before injection (including shelter positions 1 and 2 epochs) was divided into 12 bins of equal duration. Odd bins were used to train the classifier and even bins used to cross-validate it, producing the baseline prediction accuracy result. The same classifier was used to predict the behavioural variable, given spike trains, after injection of CNO or saline. This was repeated 10 times, by randomly choosing the samples of data for each class. To probe the effect of inactivation of RSP, we tested the statistical significance of the difference between the change the classifier's prediction accuracy after CNO and after saline injection, using *sign rank test*. The first 35 min after injection were discarded from these analyses.

General data analysis

Data analysis was performed using custom-written routines in Python 2.7 and MATLAB and custom code will be made available on request. Data are reported as median ± i.q.r. or mean ± s.e.m unless otherwise indicated. Statistical comparisons using the significance tests stated in the main text were made in GraphPad Prism, MATLAB, R and statistical significance was considered when $P < 0.05$. Data were tested for normality with the Shapiro–Wilk test, and a parametric test used if the data were normally distributed, and a non-parametric otherwise, as detailed in the text next to each comparison. To test whether a population of angular measures was distributed non-uniformly around the circle we used a V-test for non-uniformity of circular data[83]. The z-test for equality of proportion was used to compare proportions[84]. Unless otherwise stated, statistical difference between behavioural metrics in CNO and control experiments was computed using the following permutation test (developed in collaboration with J. Rapela, Gatsby Data Center). Two groups of mice M and N, each of numerosity *m* and *n*, were tested under a different experimental condition (e.g.: control or CNO). The test statistic computed is the difference between the mean of all trials pooled in CNO group and the mean of the trials in the control group. For the permutation, at every iteration each mouse is randomly re-assigned to CNO or control group, while keeping the total number of mice per condition the same. The N number in this statistical comparison is therefore the number of mice in each group. The procedure was repeated 100000 times and the test statistics was computed after each iteration, obtaining the null distribution of the test. The p-

value of the test is one minus the percentile of the null distribution corresponding to the value of the test statistic of the non-shuffled data.

The data that support the findings of this study are available from the corresponding authors upon request.

Acknowledgments

This work was funded by a Wellcome Senior Research Fellowship (214352/Z/18/Z) and by the Sainsbury Wellcome Centre Core Grant from the Gatsby Charitable Foundation and Wellcome (090843/F/09/Z) (T.B.), MRC PhD Studentship (R.V.), Boehringer Ingelheim Fonds PhD fellowship (R.V.), Gatsby Unit/SWC Joint Research Fellowship in Neuroscience (D.C.), UCL Wellcome 4-year PhD Programme in Neuroscience (O.P.A), A*STAR National Science Scholarship (PhD; Y.L.T) and the SWC PhD Programme (Y.L.T.). We thank members of the Branco lab and T. Mrsic-Flogel for discussions; F. Claudi for help with DeepLabCut; J. Rapela and P. Shamash for advice on statistical analysis; A. Murray, I. Duguid, C. Schimdt-Hieber, N. Burgess, M. Tripodi, and the I. Bianco lab for comments on the manuscript; M. Strom, T. Okbinoglu, R. Campbel, the SWC Neurobiological Research Facility and FabLabs for technical support; K. Betsios for programming the data acquisition software; T. R. Stones for inspiration. Source of mouse silhouettes: https://scidraw.io/.

References

1. Ellard, C. G. & Eller, M. C. Spatial cognition in the gerbil: Computing optimal escape routes from visual threats. *Anim. Cogn.* **12**, 333–345 (2009).
2. Layne, J. E., Barnes, W. J. P. & Duncan, L. M. J. Mechanisms of homing in the fiddler crab Uca rapax 1. Spatial and temporal characteristics of a system of small-scale navigation. *J. Exp. Biol.* **206**, 4413–4423 (2003).
3. Vale, R., Evans, D. A. & Branco, T. Rapid Spatial Learning Controls Instinctive Defensive Behavior in Mice. *Curr. Biol.* **27**, 1342–1349 (2017).
4. Evans, D. A. *et al.* A synaptic threshold mechanism for computing escape decisions. *Nature* **558**, 590–594 (2018).
5. Shang, C. *et al.* A parvalbumin-positive excitatory visual pathway to trigger fear responses in mice. *Science.* **348**, 1472–1477 (2015).
6. Wei, P. *et al.* Processing of visually evoked innate fear by a non-canonical thalamic pathway. *Nat. Commun.* **6**,

1–13 (2015).

7. Xiong, X. R. *et al.* Auditory cortex controls sound-driven innate defense behaviour through corticofugal projections to inferior colliculus. *Nat. Commun.* **6**, 1–12 (2015).

8. Branco, T. & Redgrave, P. The Neural Basis of Escape Behavior in Vertebrates. *Annu. Rev. Neurosci.* (2020) doi:10.1146/annurev-neuro-100219-122527.

9. Tovote, P., Fadok, J. P. & Lüthi, A. Neuronal circuits for fear and anxiety. *Nature Reviews Neuroscience* vol. 16 317–331 (2015).

10. Domenici, P., Blagburn, J. M. & Bacon, J. P. Animal escapology I: Theoretical issues and emerging trends in escape trajectories. *Journal of Experimental Biology* vol. 214 2463–2473 (2011).

11. Cooper, W. E. & Blumstein, D. T. *Escaping from predators: An integrative view of escape decisions*. *Escaping from Predators: An Integrative View of Escape Decisions* (2015). doi:10.1017/CBO9781107447189.

12. Husak, J. F. Does survival depend on how fast you can run or how fast you do run? *Funct. Ecol.* **20**, 1080–1086 (2006).

13. Etienne, A. S. & Jeffery, K. J. Path integration in mammals. *Hippocampus* **14**, 180–192 (2004).

14. van der Meer, M. A. A., Richmond, Z., Braga, R. M., Wood, E. R. & Dudchenko, P. A. Evidence for the Use of an Internal Sense of Direction in Homing. *Behav. Neurosci.* **124**, 164–169 (2010).

15. Hartley, T., Lever, C., Burgess, N. & O'Keefe, J. Space in the brain: How the hippocampal formation supports spatial cognition. *Philosophical Transactions of the Royal Society B: Biological Sciences* vol. 369 (2014).

16. Taube, J. S. The Head Direction Signal: Origins and Sensory-Motor Integration. *Annu. Rev. Neurosci.* **30**, 181–207 (2007).

17. Rowland, D. C., Roudi, Y., Moser, M.-B. & Moser, E. I. Ten Years of Grid Cells. *Annu. Rev. Neurosci.* **39**, 19–40 (2016).

18. Finkelstein, A., Las, L. & Ulanovsky, N. 3-D Maps and Compasses in the Brain. *Annu. Rev. Neurosci.* **39**, 171–196 (2016).

19. Mongeau, R., Miller, G. A., Chiang, E. & Anderson, D. J. Neural correlates of competing fear behaviors evoked by an innately aversive stimulus. *J. Neurosci.* **23**, 3855–3868 (2003).

20. Cho, J. & Sharp, P. E. Head direction, place, and movement correlates for cells in the rat retrosplenial cortex. *Behav. Neurosci.* **115**, 3–25 (2001).

21. Chen, L. L., Lin, L. H., Green, E. J., Barnes, C. A. & McNaughton, B. L. Head-direction cells in the rat posterior cortex - I. anatomical distribution and behavioral modulation. *Exp. Brain Res.* **101**, 8–23 (1994).

22. Angelaki, D. E. *et al.* A gravity-based three-dimensional compass in the mouse brain. *Nat. Commun.* **11**, 1–13 (2020).

23. Miller, A. M. P., Mau, W. & Smith, D. M. Retrosplenial Cortical Representations of Space and Future Goal Locations Develop with Learning. *Curr. Biol.* **29**, 2083-2090.e4 (2019).

24. Vedder, L. C., Miller, A. M. P., Harrison, M. B. & Smith, D. M. Retrosplenial Cortical Neurons Encode Navigational Cues, Trajectories and Reward Locations during Goal Directed Navigation. *Cereb. Cortex* **27**, 3713–3723 (2017).

25. Laurens, J. *et al.* Multiplexed code of navigation variables in anterior limbic areas. *bioRxiv* 684464 (2019) doi:10.1101/684464.

26. Mao, D., Molina, L. A., Bonin, V. & McNaughton, B. L. Vision and Locomotion Combine to Drive Path Integration Sequences in Mouse Retrosplenial Cortex. *Curr. Biol.* **30**, 1680-1688.e4 (2020).

27. Alexander, A. S. & Nitz, D. A. Retrosplenial cortex maps the conjunction of internal and external spaces. *Nat. Neurosci.* **18**, 1143–1151 (2015).

28. Cooper, B. G., Miya, D. Y. & Mizumori, S. J. Y. Superior colliculus and active navigation: Role of visual and non-visual cues in controlling cellular representations of space. *Hippocampus* **8**, 340–372 (1998).

29. Schiller, P. H. & Stryker, M. Single-unit recording and stimulation in superior colliculus of the alert rhesus monkey. *J. Neurophysiol.* **35**, 915–924 (1972).

30. Wurtz, R. H. & Goldberg, M. E. Activity of superior colliculus in behaving monkey. 3. Cells discharging before eye movements. *J. Neurophysiol.* **35**, 575–586 (1972).

31. Masullo, L. *et al.* Genetically Defined Functional Modules for Spatial Orienting in the Mouse Superior Colliculus. *Curr. Biol.* **29**, 2892-2904.e8 (2019).

32. Freedman, E. G. & Sparks, D. L. Activity of Cells in the Deeper Layers of the Superior Colliculus of the Rhesus Monkey: Evidence for a Gaze Displacement Command. *J. Neurophysiol.* **78**, 1669–1690 (1997).

33. Dean, P., Mitchell, I. J. & Redgrave, P. Responses resembling defensive behaviour produced by microinjection of glutamate into superior colliculus of rats. *Neuroscience* **24**, 501–510 (1988).

34. Sahibzada, N., Dean, P. & Redgrave, P. Movements resembling orientation or avoidance elicited by electrical stimulation of the superior colliculus in rats. *J. Neurosci.* **6**, 723–733 (1986).

35. Benavidez, N. L. *et al.* The mouse cortico-tectal projectome. *bioRxiv* 2020.03.24.006775 (2020) doi:10.1101/2020.03.24.006775.

36. Caño, G. G. Del, Gerrikagoitia, I. & Martínez-Millán, L. Morphology and topographical organization of the retrospleniocollicular connection: A pathway to relay contextual information from the environment to the superior colliculus. *J. Comp. Neurol.* **425**, 393–408 (2000).

37. van Groen, T. & Wyss, J. M. Connections of the retrosplenial dysgranular cortex in the rat. *J. Comp. Neurol.* **315**, 200–216 (1992).

38. Basso, M. A. & May, P. J. Circuits for Action and Cognition: A View from the Superior Colliculus. *Annu. Rev. Vis. Sci.* **3**, 197–226 (2017).

39. Ito, S. & Feldheim, D. A. The mouse superior colliculus: An emerging model for studying circuit formation and function. *Frontiers in Neural Circuits* (2018) doi:10.3389/fncir.2018.00010.

40. Mitchell, A. S., Czajkowski, R., Zhang, N., Jeffery, K. & Nelson, A. J. D. Retrosplenial cortex and its role in spatial cognition. *Brain Neurosci. Adv.* **2**, 239821281875709 (2018).

41. Vann, S. D., Aggleton, J. P. & Maguire, E. A. What does the retrosplenial cortex do? *Nature Reviews Neuroscience* vol. 10 792–802 (2009).

42. Burgess, N. Spatial cognition and the brain. *Annals of the New York Academy of Sciences* (2008) doi:10.1196/annals.1440.002.

43. Wickersham, I. R. *et al.* Monosynaptic Restriction of Transsynaptic Tracing from Single, Genetically Targeted Neurons. *Neuron* (2007) doi:10.1016/j.neuron.2007.01.033.

44. Tervo, D. G. R. *et al.* A Designer AAV Variant Permits Efficient Retrograde Access to Projection Neurons. *Neuron* **92**, 372–382 (2016).

45. Maguire, E. A. The retrosplenial contribution to human navigation: A review of lesion and neuroimaging findings. *Scand. J. Psychol.* (2001) doi:10.1111/1467-9450.00233.

46. Stachniak, T. J., Ghosh, A. & Sternson, S. M. Chemogenetic Synaptic Silencing of Neural Circuits Localizes a Hypothalamus→Midbrain Pathway for Feeding Behavior. *Neuron* **82**, 797–808 (2014).

47. Mohler, C. W. & Wurtz, R. H. Organization of monkey superior colliculus: intermediate layer cells discharging before eye movements. *J. Neurophysiol.* **39**, 722–744 (1976).

48. Wilson, J. J., Alexandre, N., Trentin, C. & Tripodi, M. Three-Dimensional Representation of Motor Space in the Mouse Superior Colliculus. *Curr. Biol.* **28**, 1744-1755.e12 (2018).

49. Bergeron, A., Matsuo, S. & Guitton, D. Superior colliculus encodes distance to target, not saccade amplitude, in multi-step gaze shifts. *Nat. Neurosci.* **6**, 404–413 (2003).

50. Jay, M. F. & Sparks, D. L. Sensorimotor integration in the primate superior colliculus. II. Coordinates of auditory signals. *J. Neurophysiol.* (1987) doi:10.1152/jn.1987.57.1.35.

51. Middlebrooks, J. C. & Knudsen, E. I. A neural code for auditory space in the cat's superior colliculus. *J. Neurosci.* **4**, 2621–2634 (1984).

52. Alexander, A. S. *et al.* Egocentric boundary vector tuning of the retrosplenial cortex. *Sci. Adv.* **6**, eaaz2322 (2020).

53. Jacob, P. Y. *et al.* An independent, landmark-dominated head-direction signal in dysgranular retrosplenial cortex. *Nat. Neurosci.* **20**, 173–175 (2017).

54. Alexander, A. S. & Nitz, D. A. Spatially Periodic Activation Patterns of Retrosplenial Cortex Encode Route Sub-spaces and Distance Traveled. *Curr. Biol.* (2017) doi:10.1016/j.cub.2017.04.036.

55. Sarel, A., Finkelstein, A., Las, L. & Ulanovsky, N. Vectorial representation of spatial goals in the hippocampus of bats. *Science.* **355**, 176–180 (2017).

56. Wang, C. *et al*. Egocentric coding of external items in the lateral entorhinal cortex. *Science.* **362**, 945–949 (2018).

57. LaChance, P. A., Todd, T. P. & Taube, J. S. A sense of space in postrhinal cortex. *Science.* **365**, (2019).

58. Wang, C., Chen, X. & Knierim, J. J. Egocentric and allocentric representations of space in the rodent brain. *Current Opinion in Neurobiology* vol. 60 12–20 (2020).

59. Hinman, J. R., Chapman, G. W. & Hasselmo, M. E. Neuronal representation of environmental boundaries in egocentric coordinates. *Nat. Commun.* **10**, 1–8 (2019).

60. Fecteau, J. H. & Munoz, D. P. Salience, relevance, and firing: a priority map for target selection. *Trends in Cognitive Sciences* (2006) doi:10.1016/j.tics.2006.06.011.

61. Krauzlis, R. J., Lovejoy, L. P. & Zénon, A. Superior Colliculus and Visual Spatial Attention. *Annu. Rev. Neurosci.* (2013) doi:10.1146/annurev-neuro-062012-170249.

62. Horwitz, G. D. & Newsome, W. T. Separate signals for target selection and movement specification in the superior colliculus. *Science.* **284**, 1158–1161 (1999).

63. Duan, C. A., Erlich, J. C. & Brody, C. D. Requirement of Prefrontal and Midbrain Regions for Rapid Executive Control of Behavior in the Rat. *Neuron* (2015) doi:10.1016/j.neuron.2015.05.042.

64. Inoue, K. I., Takada, M. & Matsumoto, M. Neuronal and behavioural modulations by pathway-selective optogenetic stimulation of the primate oculomotor system. *Nat. Commun.* (2015) doi:10.1038/ncomms9378.

65. Jiang, W., Jiang, H. & Stein, B. E. Two corticotectal areas facilitate multisensory orientation behavior. *J. Cogn. Neurosci.* (2002) doi:10.1162/089892902760807230.

66. Johnston, K., Koval, M. J., Lomber, S. G. & Everling, S. Macaque dorsolateral prefrontal cortex does not suppress saccade-related activity in the superior colliculus. *Cereb. Cortex* (2014) doi:10.1093/cercor/bhs424.

67. Paré, M. & Wurtz, R. H. Progression in neuronal processing for saccadic eye movements from parietal cortex area LIP to superior colliculus. *J. Neurophysiol.* (2001) doi:10.1152/jn.2001.85.6.2545.

68. Honda, Y. & Ishizuka, N. Topographic distribution of cortical projection cells in the rat subiculum. *Neurosci. Res.* **92**, 1–20 (2015).

69. Cenquizca, L. A. & Swanson, L. W. Spatial organization of direct hippocampal field CA1 axonal projections to the rest of the cerebral cortex. *Brain Research Reviews* vol. 56 1–26 (2007).

70. Armbruster, B. N., Li, X., Pausch, M. H., Herlitze, S. & Roth, B. L. Evolving the lock to fit the key to create a

family of G protein-coupled receptors potently activated by an inert ligand. *Proc. Natl. Acad. Sci. U. S. A.* (2007) doi:10.1073/pnas.0700293104.

71. Sterbing, S. J., Hartung, K. & Hoffmann, K. P. Representation of sound source direction in the superior colliculus of the guinea pig in a virtual auditory environment. *Exp. Brain Res.* (2002) doi:10.1007/s00221-001-0963-y.

72. King, A. J., Hutchings, M. E., Moore, D. R. & Blakemore, C. Developmental plasticity in the visual and auditory representations in the mammalian superior colliculus. *Nature* (1988) doi:10.1038/332073a0.

73. Ragan, T. *et al.* Serial two-photon tomography for automated ex vivo mouse brain imaging. *Nat. Methods* (2012) doi:10.1038/nmeth.1854.

74. Jun, J. J. *et al.* Fully integrated silicon probes for high-density recording of neural activity. *Nature* **551**, 232–236 (2017).

75. Jun, J. J. *et al.* Real-time spike sorting platform for high-density extracellular probes with ground-truth validation and drift correction. *bioRxiv* (2017) doi:10.1101/101030.

76. Pachitariu, M., Steinmetz, N., Kadir, S., Carandini, M. & Harris, K. D. *Kilosort: realtime spike-sorting for extracellular electrophysiology with hundreds of channels*. *bioRxiv* (2016) doi:10.1101/061481.

77. Mathis, A. *et al.* DeepLabCut: markerless pose estimation of user-defined body parts with deep learning. *Nat. Neurosci.* (2018) doi:10.1038/s41593-018-0209-y.

78. Batschelet, E. *Circular statistics in biology BT - Mathematics in biology*. (Academic Press, 1981).

79. Taube, J. S., Muller, R. U. & Ranck, J. B. Head-direction cells recorded from the postsubiculum in freely moving rats. I. Description and quantitative analysis. *J. Neurosci.* **10**, 420–435 (1990).

80. Gu, Y., Fetsch, C. R., Adeyemo, B., DeAngelis, G. C. & Angelaki, D. E. Decoding of MSTd population activity accounts for variations in the precision of heading perception. *Neuron* (2010) doi:10.1016/j.neuron.2010.04.026.

81. Campagner, D., Evans, M. H., Bale, M. R., Erskine, A. & Petersen, R. S. Prediction of primary somatosensory neuron activity during active tactile exploration. *Elife* (2016) doi:10.7554/eLife.10696.

82. Nicolelis, M. A. L. *et al.* Simultaneous encoding of tactile information by three primate cortical areas. *Nat. Neurosci.* **1**, 621–630 (1998).

83. Durand, D. & Greenwood, J. A. Modifications of the Rayleigh Test for Uniformity in Analysis of Two-Dimensional Orientation Data. *J. Geol.* (1958) doi:10.1086/626501.

84. Wilson, E. B. Probable Inference, the Law of Succession, and Statistical Inference. *J. Am. Stat. Assoc.* (1927) doi:10.1080/01621459.1927.10502953.